The Effect of Energy Components Modifications on the Crashworthiness of Thin-Walled Structures

Michał Rogala[1*], Jakub Gajewski[1]

[1] Lublin University of Technology, Faculty of Mechanical Engineering, Department of Machine Design and Mechatronics

* Corresponding author's e-mail: m.rogala@pollub.pl

ABSTRACT

Thin-walled structures that serve as energy absorbers are widely used in the automotive industry, and it is well-known that they deform in a specific way under dynamic loading, forming plastic hinges along the yield line. The dynamic impact of these structures causes various phenomena that affect the formation of folds and, consequently, the dynamic response of the structure. The force-shortening curve, which is based on the unified crush efficiency indicators, is a key factor in determining the dynamic response of the structure. While there have been many studies on energy absorbers under static or quasi-static loading conditions, the effect of changing kinetic energy components (mass and velocity) on the obtained crush efficiency indicators is not as well understood. This article presents the results of experimental tests and nonlinear numerical simulations for eleven different initial conditions of the crashworthiness analysis. The tests showed a significant effect of changing the velocity and mass of the striker on the results obtained. Additionally, the nonlinear effect of the change in the velocity of the tup with respect to the peak force and total efficiency was demonstrated.

Keywords: thin-walled structures, dynamic impact, energy absorber, FEM.

INTRODUCTION

The influence of velocity on the crashworthiness of car component deformation is very significant. Higher velocities during impacts result in greater kinetic energy, leading to more severe deformation and potentially increased risk of injury to occupants [1,2]. However, controlled deformation is crucial for dissipating energy and reducing the impact forces transferred to the occupants. Engineers design car components, such as bumpers, crumple zones, and safety cages, to effectively absorb and distribute energy across the vehicle structure, regardless of impact velocity. Advanced materials and structural designs, including composite sandwich structures, are employed to optimize crashworthiness across a range of velocities, ensuring the safety of occupants in various collision scenarios. Crash analysis is of huge importance in identifying effective solutions for protecting passengers from serious injury and determining optimal methods for minimizing the damage sustained by a vehicle during a collision with an obstacle or another vehicle. An important area of interest for researchers in this field is reducing the impulsive impact on the driver, which is often caused by the immediate reaction forces generated by these obstacles [3]. Thin-walled aluminum alloy structures are of significant importance in several industries due to their high energy absorption capabilities and lightweight design. These structures are primarily employed in the aerospace and automotive sectors. The various cross-sectional shapes of these structures, including square and hexagonal, have been extensively documented [4–7]. Thin-walled tubular elements are considered to be the best energy-absorbing structures for a complex load condition [8,9]. Particularly widely addressed in the articles is the issue of stability and failure of

composite structures with open or closed cross sections [10–12].

Thin-walled columns subjected to axial force are often disturbed by geometric imperfection that allows to lower peak force values especially dangerous in the first phase of crushing [13–15]. The study shows the influence of different types of initiators on the values of generated overload during the formation of the first plastic hinge. It is noteworthy that the manner of initiation of the crush through its initiation by disturbing the geometry of the column also affects the manner of plastic deformation in the further stage of the crush [16,17]. Triggers also influence the formation of plastic deformation of the column in the case of oblique impact. Santhosh et al. conducted a research on oblique impact of the angles of 15°, 30° and 45° [18].

The examination of current research demonstrates a rising trend in the incorporation of bioinspired concepts during the design process for the configurations of the cross-sectional shapes and profiles of passive energy absorbers [19, 20]. Researchers see the application of artificial neural networks and machine learning for structural optimization, as well as the assessment of the energy-absorbing capacity of engineering structures [21–24]. Ma et al. proposed an algorithm to determine crush efficiency indices as well as optimize the thin-walled structure [25]. Zhang et al. were inspired by the unique doubly symmetrical structure of dragonfly wings, a set of multicellular elliptical tubes (METs) designed to enhance the energy absorption capacity of thin-walled tubes under various loading scenarios. The results suggest that the performance of METs under crashworthiness conditions may be affected by the number of basic corner elements. Moreover, METs show greater energy absorption capacity during diagonal compression as opposed to axial compression [26]. As a result of the design of structures and unusual shapes, researchers of scientific papers use various manufacturing technologies, including 3D printing (metal powder sintering) and other additive techniques [27, 28]. To optimize the energy absorption capacity of composite structures, a variable thickness hybrid multi-cell tube composed of Carbon Fiber Reinforced Plastic and aluminum has been proposed by Liang et al. The design strategies of this tube emphasize the use of variable thickness filament winding and multi-cell layout [29]. The development of a numerical modelling allowing to obtain a high-quality solution is currently possible owing to advanced computational algorithms Implicit and Explicit realizing problems based on the finite element method [30–35]. These computational algorithms make it possible to accurately determine the failure mechanism in a complex loading condition [36–38].

The crashworthiness analysis of energy-absorbing structures is carried out under different loading conditions. The authors often use static or quasi-static loading of the systems, which translates into results. Studies presented in numerous publications show that the values of reaction forces as well as overloads are derived from the velocity of forcing. An analysis of the literature also show that the velocity of the ram affects both the manner of initiation and propagation of crushing of thin-walled columns. On the basis of the publications describe in this section, the topic where is a relationship between the change in kinetic energy components on the achieved crush rates is proposed. Due to the large non-linearities caused by plastic deformation, the strain rate of the material as well as the forming plastic hinges, it is necessary to analyze the crush for constant kinetic energy with different velocity and mass components.

CRASHWORTHINESS INDICATORS

To accurately evaluate the performance of passive energy absorbers during crushing, it is crucial to employ indicators that unequivocally define the structure's performance. These indicators enable a meaningful comparison of structures discussed in literature and help determine the efficiency improvement of the structure. Over the years, researchers have identified various crush efficiency indicators based on the deformation mechanism of tubular energy absorbers [39,40]. The fundamental representation of passive energy absorbers' results is a plot of force against shortening, upon which the following crush efficiency indicators have been determined.

Energy absorption during crushing is the most fundamental quantity to consider. It is defined as the area under the characteristic function within the range of compression, and can be calculated using the following formula 1:

$$EA(x) = \int_0^\delta F(x)dx \qquad (1)$$

The mean crushing force (MCF) is derived from the energy absorbed and the crushing distance. It is given by the subsequent formula 2:

$$MCF = \frac{EA(\delta)}{\delta} \tag{2}$$

Force-crushing characteristics show the course of dynamic analysis, and also allow for determining the value of the mean (MCF) and maximum crushing force (PCF). Knowing these two basic values allows for evaluating the crushing load efficiency (CLE) by dividing the above-mentioned forces. This quantity is the fundamental parameter for determining crushing efficiency and is represented by the following Equation 3:

$$CLE = \frac{MCF}{PCF} \tag{3}$$

The stroke efficiency ratio (SE) determines the shortening of the specimen occurred during crushing in comparison with the initial length of the absorber 4:

$$SE = \frac{\delta}{L_o} \tag{4}$$

The total efficiency (TE) is the product of the two indices described above (CLE and SE), responsible for the crushing and shortening force efficiency of the sample, respectively. Using one indicator, it is possible to estimate the ability of the sample in dynamic tests, as the indicator increases, its performance improves 5:

$$TE = CLE \times SE \tag{5}$$

MATERIALS AND METHODOLOGY

The study of passive energy absorbers was carried out by dynamically crushing the structure in an Instron Ceast 9350 HES drop tower. An alternative method was using the finite element method to model the crushing phenomenon of a thin-walled column. This study is not standardized and the conditions of the conducted analyses are based on the working environment of thin-walled structures described in more detail in this section. Numerical simulations were performed using Abaqus CAE software. The subjects of the study were thin-walled columns subjected to a kinetic energy of 1700 J. The tests were implemented for columns made of AA-6063 T6 aluminum

with constant geometrical parameters. The column had a height of 200 mm, a cross section of 40×40 mm and a wall thickness of 1.2 mm. The energy absorbers were disrupted with a crush initiator in the form of spherical embossments with a diameter of 32 mm and a depth of 3.6 mm. As the crush initiator, it is understood that two of four embossments, are convex while another two are concave. The shape of the triggers corresponds to the symmetrical form of the plastic hinge characteristic of square energy absorbers.

$$E_k = \frac{mv^2}{2} \tag{6}$$

The subject of the present analysis was to determine the effect of changing the kinetic energy components on the achieved crush efficiency indicators. The study was carried out for 11 configurations shown in Table 1. The changes in mass values varied in the range of 20–120 kg every 10 kg. The velocity component was determined from the kinetic energy formula 6. In the experimental studies, validation was carried out for one selected initial condition, i.e. S6. Due to the working conditions of the passive energy absorbers in vehicle motors, i.e. protection of vehicle components at velocities up to 25 km/h, these initial conditions were selected

The subjects of the research were column absorbers made of AA-6063-T6 alloy. The absorbers were made using thin-walled aluminum profiles supplied by Sapa Company of Chrzanow, Poland. The aluminum alloy applied is AA-6063-T6, which is characterized by high ductility and strength, which is crucial considering the manner of deformation of road energy absorbers. The main alloy additives are manganese and silicon, and the entire chemical composition is shown in Table 2. The table also includes selected mechanical properties, which served as a reference during the selection of the material. The main analysis of the mechanical properties of the aluminum alloy was carried out on a split Hopkinson pressure bar stand and the results are shown in Table 3.

A crucial concern regarding energy absorbers involves the theoretical aspects of stress and shock waves, which arise from the dynamic

Table 1. Comparison of kinetic energy components for the analyzed cases

Name	S1	S2	S3	S4	S5	S6	S7	S8	S9	S10	S11
Mass [kg]	20	30	40	50	60	70	80	90	100	110	120
Velocity [m/s]	13.04	10.65	9.22	8.25	7.53	6.97	6.52	6.15	5.83	5.56	5.32

Table 2. Technical parameters of aluminum alloy suitable for column absorbers

Name	EN AA 6063 T6						
Chemical composition [%]	Si	Fe	Cu	Mn	Mg	Zn	Ti
	0.54	0.23	0.008	0.051	0.481	0.005	0.021
Heat treatment	8 hours at 198 °C						
Mechanical properties*	Re [MPa]		Rm [MPa]		A50 [%]		Brinell hardness
	240		265		11.5		80

Table 3. Parameters of the Johnson-Cook plastic material model

Symbol	Name	Unit	Value
A	Yield stress	MPa	240
B	Strain hardening coefficient	MPa	1923
n	Strain hardening exponent	–	1.8
C	Strain rate sensitivity	–	0.001
m	Thermal softening coefficient	–	0

nature of the process [41–43]. For the analysis of crashworthiness, the influence of a material's sensitivity to strain rate is commonly acknowledged. Hopperstad et al. [44–46] provide a comprehensive explanation of these phenomena, where a thorough examination of the constitutive material model for aluminum alloys is presented. During the numerical simulation of the issue using the finite element method, the plastic material properties were described using the Johnson-Cook model (7).

$$\sigma(\varepsilon, \dot{\varepsilon}, T) =$$
$$\left[A + B\left(\bar{\varepsilon}^{pl}\right)^n \right]\left(1 + C \ln\left(\frac{\dot{\bar{\varepsilon}}^{pl}}{\dot{\varepsilon}_0}\right) \right)\left(1 - \left(\frac{T - T_R}{T_m - T_R}\right)^m \right) \quad (7)$$

Considering the stated thesis and evaluating the effect of changing the velocity and mass components of kinetic energy, the previously verified Johnson-Cook plastic model was used in the numerical analyses. The model's values in the plastic range were determined by an experimental study on a split Hopkinson pressure bar stand. On a basis of the stress-strain curves at different velocities of the bar, the indicators' characteristics for the Johnson-Cook model were determined, as presented below in Table 3. The methodology for this research involves both experimental testing and numerical simulations. The Instron Ceast 9350HES drop tower and the Abaqus program were utilized to conduct advanced simulations. The study utilized samples with configuration of initial parameters S6, as detailed in Table 1. The experimental testing included both qualitative and quantitative comparisons of the results obtained from the simulations using the finite element method. The crushing process was recorded through the use of a piezoelectric sensor, which collected the reaction force and presented the results on a force-shortening diagram. The initiation and propagation of the crushing process was documented through the use of a time-lapse camera, the Phantom Miro M310. Graphical representations of the plastic hinge formation were compiled from the different stages of the crushing process, along with the figures from the numerical analysis. The sampling frequency of the sensor was specified as 100 kHz, which, with respect to the duration of one crush (30–45 ms), allows to obtain 4000 measurement points. The number of points obtained is extremely important due to the rapid changes in the response of the thin-walled structure resulting from forming plastic hinges.

To ensure the accuracy of the conducted analyses, a mesh convergence analysis was performed (Figure 1). The study utilized seven different column finite element sizes, ranging from 1–4 mm with increments of 0.5 mm. The reaction forces were then compared to the experimental results. The mesh convergence analysis indicated that the most suitable finite element size for the FEM analyses was 1.5 mm, as this size produced the highest convergence of results. The evaluation criteria for this analysis included the location of the force peaks and the duration of the analysis.

The numerical simulation was developed with the purpose of reproducing the bench tests as accurately as possible. The problem was

Figure 1. Finite element sizes

modeled based on two types of finite elements. A thin-walled column was made using shell elements (S4) with a linear shape function having four integration points. Another type of element assigned to the plate serving as the base and striker was a non-deformable shell element (R3D4) characterized by a linear shape function and four integration points for the finite element. The finite elements had six degrees of freedom (three rotational and three translational) according to the scheme in Figure 2. The linear shape function of the finite elements resulted from the

Explicite computational solver used. The computational algorithm is based on the kinematic equations of motion 8:

$$\dot{u}^N_{\left(i+\frac{1}{2}\right)} = \dot{u}^N_{\left(i-\frac{1}{2}\right)} + \frac{\Delta t_{i+1} + \Delta t_i}{2} \ddot{u}^N_{(i)} \qquad (8)$$

where: u^N is a degree of freedom (displacement and rotation), and i is an increment related to step in explicit dynamic.

Using the explicit integration method, it is not possible to use the quadratic finite element shape function. The adopted method of solving the
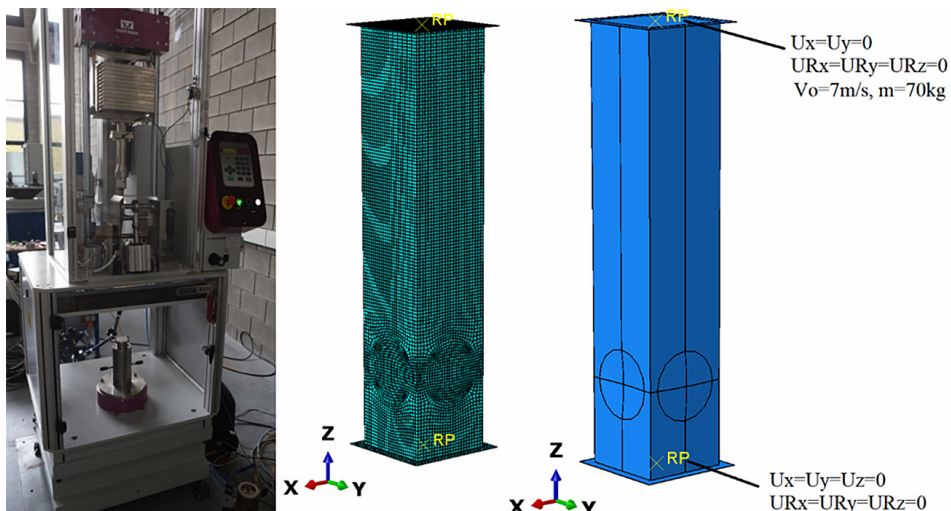

Figure 2. Experimental stand with corresponding conditions of numerical analysis (a) instron drop tower (b) discretized model (c) boundary condition of numerical simulation

problem is characterized by high computational rate and high accuracy while maintaining certain criteria for time increment stability. The computational algorithm solves the problem in a finite interval. The determined values are the initial state for the next computational step. According to the Abaqus software documentation [47] the stability criterion of the computational step increment is the time sufficient to traverse the stress wave through the smallest finite element 9:

$$\Delta t \leq \frac{2}{\omega_{max}}(\sqrt{1 + \xi_{max}^2} - \xi_{max}) \qquad (9)$$

where: ξ_{max} is the fraction of the critical damping, L_{max} the dimension of the smallest element of mesh, and C_d is the dilatation wave speed specified for materials

RESULTS

This section presents the results of the bench tests and numerical simulations, which are expressed in the form of force-shortening curves and crush efficiency indicators. Additionally, a comparative graphical analysis was made on the formation of plastic hinges based on high-speed camera images at different stages of dynamic crushing. Experimental verification was performed for the samples with designation S6 (Table 1).

Based on the curves in Figure 3, it can be seen that the value of velocity translates into the manner in which the first and second folds are formed. The effect can be seen in the first crush phase up to 50 mm of shortening. At lower beater velocity, the force peak is lower and the second plastic joint is shaped around 45 mm, which is evident by the increase in the force value. In

the case of S7-S11 specimens, as a result of the increased value of the beater velocity, there is a deflection in the formation area of the second plastic hinge to 30 mm of shortening of the thin-walled column. It is worth noting that the total shortening of the columns in all cases is about 140 mm. The difference in total shortening between the cases is negligible.

The figures below (Figs. 4–6) illustrate the efficiency indicators of passive energy absorbers for crushing. The values of these indices were calculated based on the numerical simulations performed using the finite element method outlined in Section 3. The method for determining these indicators and their definitions are described above. These indices are commonly utilized in the literature for the authoritative assessment of the potential of thin-walled structures. Additionally, they are employed to evaluate and compare the performances of various structures that have undergone crushing, specifically through the formation of successive plastic hinges.

The first indicator's value vary between 27 and 38 kN. The lowest value of this indicator was observed in sample S11, which also had the lowest velocity component for a given kinetic energy. Despite the constant kinetic energy, there is a non-linear change in the indicators due to the change in the components. Another indicator that clearly demonstrates the effect of striker velocity on the performance of a passive energy absorber is CLE. As shown in Figure 5, the efficiency of the crushing force changes with the variations of the striker velocity, and the index ranges from 0.33–0.47, showing an increase of approximately 40%. In the case of the described issue, this increase is crucial for clearly
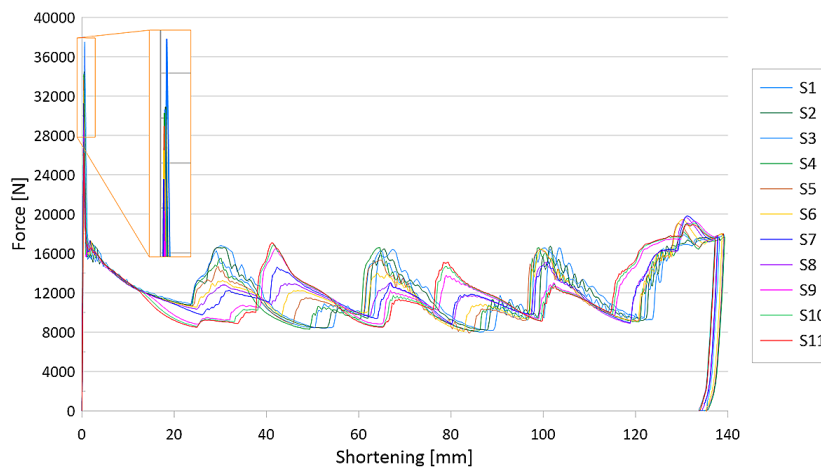

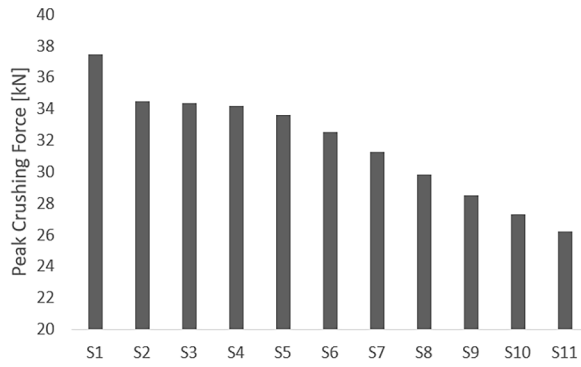**Figure 3.** Force-shortening curve for column with different initial condition

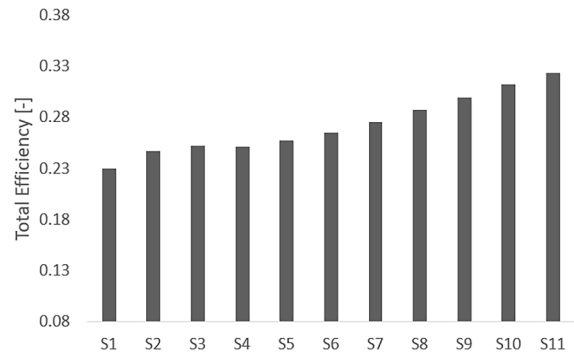**Figure 4.** PCF indicators for all analyzed cases (FEM)

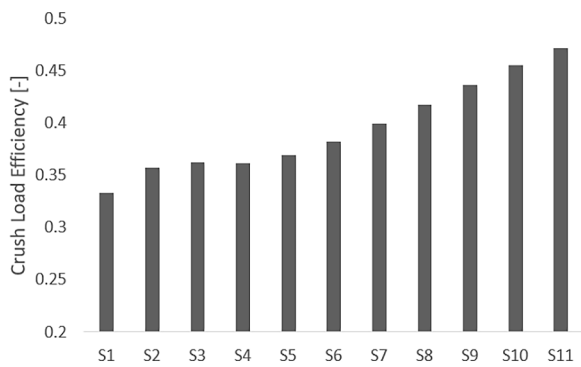**Figure 6.** TE indicators for all analyzed cases (FEM)

Figure 5. CLE indicators for all analyzed cases (FEM)

determining the performances of the analyzed structures. The last presented indicator, TE, has a value that ranges from 0.23-0.33, representing an increase of nearly 50%.

The verification of the numerical analyses was carried out using an Instron Ceast 9350 HES dynamic test stand. Experimental tests were performed on three S6 specimens with specified initial conditions, including a 70 kg striker mass and a striker velocity of 6.97 m/s. The results of the tests were presented in the form of force-shortening curves (Figure 7), graphical presentation of the
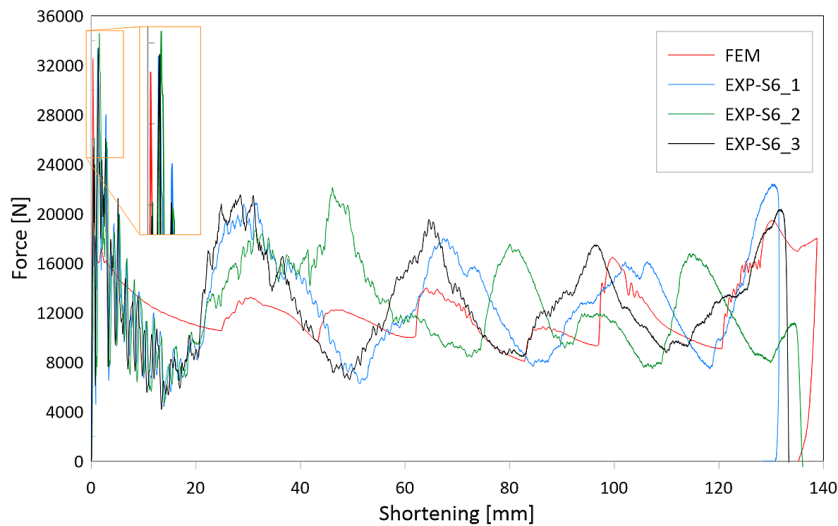

Figure 7. Force-shortening curves for three S6 samples compared with the results of the FEM analysis

Table 4. Comparison of the crashworthiness indicator from the experiment and numerical simulation

Name	δ (mm)	PCF (kN)	MCF (kN)	CLE (-)	SE (-)	TE (-)
32-3.6-1-S1	131.53	33.330	12.959	0.389	0.658	0.256
32-3.6-1-S2	136.03	34.565	12.614	0.365	0.680	0.248
32-3.6-1-S3	133.38	33.419	12.889	0.386	0.667	0.257
FEM	139.55	33.563	12.358	0.368	0.698	0.257
Difference [%]	4.23	0.62	3.74	3.15	4.23	1.24

forming folds (Figure 8), and crush efficiency indicators (Table 4). This presentation of the results allowed for both quantitative and qualitative verifications and validations of the numerical results.

The force waveform in the graph below (Figure 7) displays a high degree of agreement between the characteristics, particularly for specimens S1 and S3. In the analyzed curves, it can be seen that plastic hinges form at 30 mm, 65 mm, 100 mm, and 135 mm. The crushing mechanism is characterized by a symmetrical form, which is typical of thin-walled columns with a square cross-section. In the case of experimental specimen S2, it is notable that the force peak corresponding to the second plastic joint is broken into

two smaller ones (Figure 7). Time-lapse analysis did not reveal the presence of crush misalignment (Figure 9). The formed folds are symmetrical about the column axis, which is characteristic of passive energy absorbers with a crush initiator in the form of a spherical embossment.

The determined crush efficiency ratios of embossments of significant diameter and depth are characterized by a slight difference with respect to the results of numerical simulations. The errors do not exceed 5% in any case (Table 4), noting that the peak force value obtained for individual S1–S3 specimens vary in the range of 2–3 kN, and the obtained order of magnitude is repeatable. Numerical analysis shows lower values of the PCF index
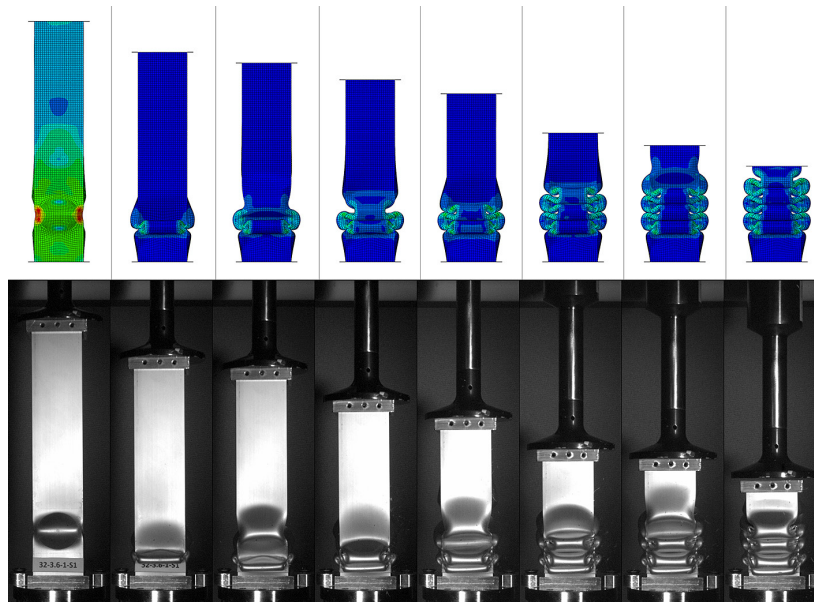

Figure 8. Graphical analysis of the initiation and propagation of the dynamic crush process
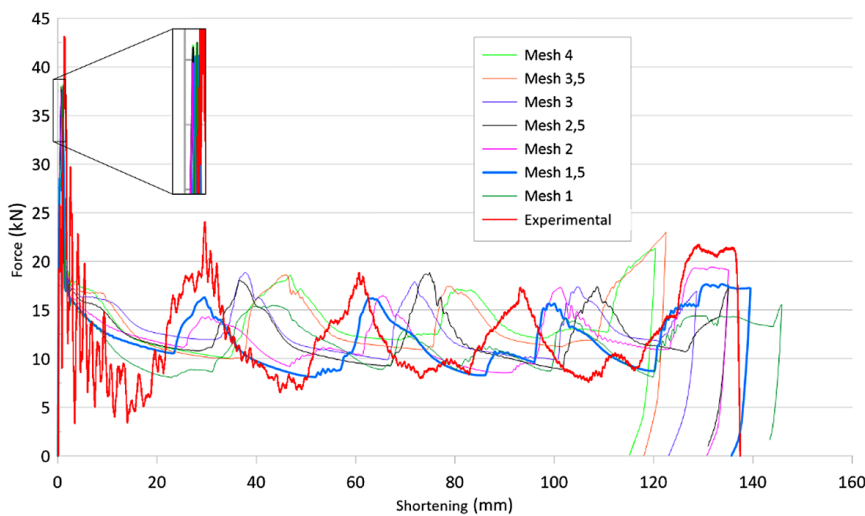

Figure 9. Time-lapse analysis of crush process

for all models which may be related to the isotropic mechanism of aluminum alloy strengthening in the assumed plastic model [48]. The reason for the discrepancy in the obtained results may be the concentration of stresses within the crush initiator. The mechanism of producing spherical embossing in the strengthening of the structure, resulting in an increased force peak (PCF). As a result of static overstressing of the material and accompanying plastic deformation, the directional orientation and shape of the grains change [49, 50].

Other characteristic quantities describing the crush of the S6 model did not show increased difference. Both the shortening of the samples and the value of the average crushing force revealed an discrepancies of about 3%. The intermediate indices derived from the PCF show an error at a gently increased level, noting that the S6 model had a high level of agreement, as evidenced by the crush course seen in Figures 7 and 8.

CONCLUSIONS

The article discusses the impact of velocity on the crashworthiness of car components and ways of the engineers design structures to optimize energy absorption capacity. Thin-walled structures, such as aluminum alloy structures, are important in several industries due to their energy absorption capabilities and lightweight design. The study examines the influence of initiators on the generation of overload during the formation of the first plastic hinge and the manner of plastic deformation in further stages of crushing. The article presents the influence of different components of kinetic energy. Specimens were tested with the same kinetic energy however with different velocity and mass of stricker. The effect of velocity change was observed in this study. The results presented in the study led to the following conclusions:

1. The use of different kinetic energy components for numerical simulations is closely related to determining the energy-absorption performance of columnar structures,
2. The use of static or quasistatic tests affects the reduction of overloads recorded during the testing of passive energy absorbers. The manner of plastic deformation of the structure is closely related to the initial conditions of the analysis, and therefore it is not possible to unambiguously determine the behavior of the structure in dynamic impact,
3. The changes in crush efficiency ratios are nonlinear with respect to the velocity and mass components of kinetic energy,
4. Due to the significant nonlinearities in the crush analysis of passive energy absorbers, it is recommended to use a material model considering the strain rate sensitivity as well as the material hardening resulting from progressive deformation,
5. The current research shows that the use of a spherical crush initiator stabilizes the crush of thin-walled columns; however, possible work hardening of the material within the embossments was found during the test. In order to properly represent the behavior of the material model in numerical simulations, it is recommended to use kinematic or anisotropic material hardening.

REFERENCES

1. Ratajczak M, Ptak M, Dymek M, Kubacki R, de Sousa RJA, Sbriglio C, Kwiatkowski A. Computational modelling and biomechanical analysis of age-related craniocerebral injuries: Insights into bridging veins. Appl. Sci. 2024;14:2681.

2. Ptak M, Dymek M, Sawicki M, Fernandes F.A.O, Wnuk M, Wilhelm J, Ratajczak M, Witkowska D, Kwiatkowski A, Poźniak B, Kubicki K, Tikhomirov M, Druszcz A Chybowski L. Experimental and computational approach to human brain modelling – aHEAD. Arch. Civ. Mech. Eng. 2023; 23:1–18.

3. Alardhi M, Sequeira R, Fahed M, Alrajhi J, Alkhulaifi K. Assessing the crashworthiness analysis on frontal and corner impacts of vehicle on street poles using FEA. Appl. Sci. 2022; 12.

4. Li K, Feng Y, Gao Y, Zheng H, Qiu H. Crashworthiness optimization design of aluminum alloy thin-walled triangle column based on bioinspired strategy. Materials (Basel). 2020; 13: 666.

5. Rogala M, Gajewski J, Górecki M. Study on the effect of geometrical parameters of a hexagonal trigger on energy absorber performance using ANN. Materials (Basel). 2021; 14: 5981.

6. Rogala M, Gajewski J, Ferdynus M. The effect of geometrical non-linearity on the crashworthiness of thin-walled conical energy-absorbers. Materials (Basel). 2020; 13: 4857.

7. Al-Abbas B, Abdul Rasoul ZMR, Hasan D, Rasheed SE. Experimental study on ultimate strength of steel tube column filled with reactive powder concrete. Civ. Eng. J. 2023; 9: 1344–1355.

8. Ge J, Luo T, Qiu J. Experimental investigation of the dynamic responses of thin-walled and foam-filled steel tubes subjected to repeated impacts. Materials

(Basel). 2024; 17: 1018.

9. Wan L, Hu D, Zhang H. Crashworthiness study of aluminum foam-filled tubular lattice structures based on triply periodic minimal surface metamaterials under lateral crushing. Thin-Walled Struct. 2024; 197: 111616.

10. Wysmulski P. Numerical and experimental study of crack propagation in the tensile composite plate with the open hole. Adv. Sci. Technol. Res. J. 2023; 17: 249–261.

11. Wysmulski P, Mieczkowski G. Influence of size of open hole on stability of compressed plate made of carbon fiber reinforced polymer. Adv. Sci. Technol. Res. J. 2024; 18: 238–247.

12. Rozylo P, Rogala M, Pasnik J. Buckling analysis of thin-walled composite structures with rectangular cross-sections under compressive load. Materials (Basel). 2023; 16.

13. Rogala M, Gajewski J. Crashworthiness analysis of thin-walled square columns with a hole trigger. Materials (Basel). 2023; 16: 4196.

14. Ferdynus M, Gajewski J. Identification of crashworthiness indicators of column energy absorbers with triggers in the form of cylindrical embossing on the lateral edges using artificial neural networks. Eksploat. i Niezawodn. 2022; 24: 805–821.

15. Ming S, Zhou C, Li T, Song Z, Wang B. Energy absorption of thin-walled square tubes designed by kirigami approach. Int. J. Mech. Sci. 2019; 157–158: 150–164.

16. Rogala M, Gajewski J. Analysis of the triggering mechanism of the square thin-walled absorber. Adv. Sci. Technol. Res. J. 2023;17: 206–216.

17. Wu Y, Fang J, He Y, Li W. Crashworthiness of hierarchical circular-joint quadrangular honeycombs. Thin-Walled Struct. 2018; 133: 180–191.

18. Santhosh Kumar V, Manikandaraja G. Numerical study on energy absorbing characteristics of thin-walled tube under axial and oblique impact. Alexandria Eng. J. 2016; 55: 187–192.

19. Yang W, Meyers MA, Ritchie RO. Structural architectures with toughening mechanisms in Nature: A review of the materials science of Type-I collagenous materials. 2019.

20. Doodi R, Gunji B.M. Prediction and experimental validation approach to improve performance of novel hybrid bio-inspired 3D printed lattice structures using artificial neural networks. Sci. Rep. 2023; 13: 1–17.

21. Xing J, Zhao J, Niu Q, Zhang T, Zhang C, Zhang Y, Wang W, Yan S, Lu X. Crashworthiness design and optimization of bamboo-inspired tube with gradient multi-cells. Thin-Walled Struct. 2023; 191: 111034.

22. Mohammed Sahib M, Kovács G. Multi-objective optimization of composite sandwich structures using artificial neural networks and genetic algorithm.

Results Eng. 2024; 21.

23. Gao Y, Chen X, Wei Y. Graded honeycombs with high impact resistance through machine learning-based optimization. Thin-Walled Struct. 2023; 188: 110794.

24. Rogala M, Tuchowski W, Czarnecka-Komorowska D, Gawdzińska K. Analysis and assessment of aluminum and aluminum-ceramic foams structure. Adv. Sci. Technol. Res. J. 2022; 16: 287–297.

25. Ma W, Almasifar N, Amini R, Ourang A, Mahariq I, Alhoee J. Crashworthiness evaluation and optimization of full polypropylene sandwich tubes under low-velocity impact based on machine learning algorithms. Structures 2024; 60: 105901.

26. Zhang J, Wu C, Gao Q, Zhang K, Wang L, Wang T, Ma Ch, Qiu R. Crashworthiness analysis of dragonfly inspired tubes under multiple load cases. Int. J. Mech. Sci. 2024;271:109085.

27. Andrew JJ, Alhashmi H, Schiffer A, Kumar S, Deshpande VS. Energy absorption and self-sensing performance of 3D printed CF/PEEK cellular composites. Mater. Des. 2021; 208: 109863.

28. Bogahawaththa M, Mohotti D, Hazell P.J, Wang H, Wijesooriya K, Lee CK. Energy absorption and mechanical performance of 3D printed Menger fractal structures. Eng. Struct. 2024; 305: 117774.

29. Liang H, Liu B, Pu Y, Sun H, Wang D. Crashworthiness analysis of variable thickness CFRP/Al hybrid multi-cell tube. Int. J. Mech. Sci. 2024; 266: 108959.

30. Jonak J, Karpiński R, Wójcik A. Numerical analysis of undercut anchor effect on rock. J. Phys. Conf. Ser. 2021; 2130: 012011.

31. Jonak J, Karpiński R, Wójcik A. Numerical analysis of the effect of embedment depth on the geometry of the cone failure. J. Phys. Conf. Ser. 2021; 2130: 012012.

32. Wysmulski P, Falkowicz K, Filipek P. Buckling state analysis of compressed composite plates with cutout. Compos. Struct. 2021; 274: 114345.

33. Wysmulski P, Debski H, Falkowicz K. Sensitivity of compressed composite channel columns to eccentric loading. Materials (Basel). 2022; 15: 6938.

34. Jonak J, Karpiński R, Wójcik A. Influence of anchor depth and friction coefficient between anchor and rock on the trajectory of rock masses detachment. Adv. Sci. Technol. Res. J. 2023; 17: 290–298.

35. Jonak J, Karpiński R, Wójcik A, Siegmund M. The effect of undercut anchor diameter on the rock failure cone area in pullout tests. Adv. Sci. Technol. Res. J. 2022; 16: 261–270.

36. Gjukaj A, Salihu F, Muriqi A, Cvetanovski P. Numerical behavior of extended end-plate bolted connection under monotonic loading. HighTech Innov. J. 2023; 4: 294–308.

37. Both I, Burca M, Benzar S, Ungureanu V. Numerical study on the behaviour of built-up cold-formed steel corrugated web beams end connections. Civ. Eng.

J. 2023; 9: 770–786.

38. Rogala M, Gajewski J, Gawdzińska K. Crashworthiness analysis of thin-walled aluminum columns filled with aluminum–silicon carbide composite foam. Compos. Struct. 2022; 299: 116102.

39. Pugsley A. The large-scale crumpling of thin cylindrical columns. Q. J. Mech. Appl. Math. 1960; 13: 1–9.

40. Wierzbicki T, Sinmao M.V. A simplified model of Brazier effect in plastic bending of cylindrical tubes. Int. J. Press. Vessel. Pip. 1997;

41. Jones N. Several phenomena in structural impact and structural crashworthiness. Eur. J. Mech. A/ Solids 2003; 22: 693–707.

42. Meyers M.A. Dynamic Behavior of Materials [Internet]. San Diego: John Wiley&Sons; 1994.

43. Szuladziński G. Formulas for Mechanical and Structural Shock and Impact. 2009.

44. Hoang N.H, Hopperstad O.S, Myhr O.R, Marioara C, Langseth M. An improved nano-scale material model applied in axial-crushing analyses of square hollow section aluminium profiles. Thin-Walled Struct. 2015; 92: 93–103.

45. Frodal B.H, Dæhli L.E.B, Børvik T, Hopperstad O.S. Modelling and simulation of ductile failure in textured aluminium alloys subjected to compression-tension loading. Int. J. Plast. 2019; 118: 36–69.

46. Qvale K, Hopperstad O.S, Morin D, Børvik T. Micromechanics-based simulation of quasi-static and dynamic crushing of double-chamber 6000-series aluminium profiles. Int. J. Impact Eng. 2023; 180: 104636.

47. Abaqus HTML Documentation.

48. Qin J, Holmedal B, Hopperstad O.S. A combined isotropic, kinematic and distortional hardening model for aluminum and steels under complex strain-path changes. Int. J. Plast. 2018; 101: 156–169.

49. Chen X, Chen H, Ma S, Chen Y, Dai J, Bréchet Y, Ji G, Zhong S, Wang H, Chen Z. Insights into flow stress and work hardening behaviors of a precipitation hardening AlMgScZr alloy: Experiments and modeling. Int. J. Plast. 2024; 172: 1–24.

50. Aune S, Morin D, Langseth M, Clausen A.H. Experimental and numerical study on the tensile ductility of an aluminium alloy with heat-affected zones. Eur. J. Mech. A/Solids 2024; 105: 105239.